



## Pool boiling heat transfer enhancement with segmented finned microchannels structured surface

Rinku Kumar Gouda, Manabendra Pathak\*, Mohd. Kaleem Khan

Sustainable Energy Research Lab (SERL), Indian Institute of Technology Patna, Bihta, Patna 801103, India



### ARTICLE INFO

#### Article history:

Received 26 January 2018

Received in revised form 18 June 2018

Accepted 22 June 2018

#### Keywords:

Pool boiling

Heat transfer coefficient

Heat transfer enhancement

Structured surface

Microchannels

Segmented finned microchannels

CHF

### ABSTRACT

An experimental investigation has been carried out to investigate pool boiling heat transfer characteristics of segmented finned (SF) microchannels structured surface and compare its performance with that of uniform cross-section (UCS) microchannels structured surface and plane surface. All three surfaces have been fabricated on individual copper block with a foot print area of  $10 \times 10 \text{ mm}^2$ . Pool boiling experiments have been performed with these surfaces in atmospheric pressure condition using deionized water. Experiments have been performed for applied effective heat flux range of  $0\text{--}200 \text{ W/cm}^2$ . Both the structured surfaces show better heat transfer performance compared to plane surface. It has been observed that SF structured surface shows a heat transfer improvement up to a factor of 3 times the heat transfer coefficient in plane surface whereas uniform UCS structured surface shows the improvement by a factor of 2 times the heat transfer coefficient in plane surface. Thus segmented finned microchannels structured configuration shows better heat transfer performance compared to other two surfaces. The reason behind the heat transfer improvement in SF configuration might be due to more number of active nucleation sites, better rewetting phenomenon and favorable bubble growth and release mechanism.

© 2018 Elsevier Ltd. All rights reserved.

### 1. Introduction

Due to simplicity and passive operation, pool boiling is used as an effective means of heat transfer in several applications such as nuclear reactor, electronic cooling, steam power plant, and process industries. Among different parameters, characteristics of heating surface largely affect the heat transfer rate in pool boiling. Surface morphology controls the nucleation site and wetting behavior which essentially control the heat transfer mechanism in pool boiling [1–3]. During last several decades extensive research works have been undertaken for exploring different techniques of surface modification for enhancing pool boiling heat transfer rate. Broadly these techniques can be classified into four main categories: surface area enhancement, surface roughness, surface wettability and separate liquid-vapor pathway [3–18].

In surface area enhancement technique plain heated surface is modified to increase the heat transfer area. Kandlikar and his group [3,4] performed pool boiling experiments by modifying the heated surface into a structured microchannels surface which enhanced the heat transfer area. They observed that in microchannels structured surface, bubbles nucleate from the bottom of the channel,

slide along the wall of the channel and then grow at the top of the channels to the required size followed by departure from the top wall. Since the bubbles grow at the top of the channel, therefore most parts of the surface remain flooded with the working fluid, which is the main reason for the enhancement of critical heat flux (CHF) and heat transfer coefficient. Bubble dynamics plays an important role in heat transfer enhancement of pool boiling with structured microchannels, similar to its role in flow boiling in diverging channels and channels with pin fin [19,20]. Umesh and Raja [5] introduced square shaped fins in plain surface for heat transfer enhancement in pool boiling.

Heat transfer enhancement in pool boiling has also been reported by increasing number of nucleation sites, roughening the heating surface or by incorporating porous coatings. Creation of artificial nucleation sites decreases the temperature required for onset of nucleate boiling, which helps in generating large amount of vapor bubbles. Due to generation of large amount of vapor bubbles, the bubble departure time decreases and ultimately results in heat transfer enhancement. Benjamin and Balakrishna [6] investigated the effect of surface roughness on different materials and boiling liquids. They observed that nucleation site density depends on surface roughness, wall superheat, thermo-physical properties of the liquid. Porous coatings have also been used for enhancing heat transfer by increasing nucleation sites. Patil and

\* Corresponding author.

E-mail address: [mpathak@iitp.ac.in](mailto:mpathak@iitp.ac.in) (M. Pathak).

## Nomenclature

$q''$	heat flux ( $\text{W}/\text{cm}^2$ )
$T$	temperature ( $^\circ\text{C}$ )
$g$	gravitational constant ( $\text{m}/\text{s}^2$ )
$k$	thermal conductivity ( $\text{W}/\text{mK}$ )
$h$	heat transfer coefficient ( $\text{w}/\text{m}^2\text{K}$ )
$W$	width of microchannels (mm)
$D_h$	hydraulic diameter (mm)
$I$	applied current (A)
$V$	voltage

## Greek symbols

$T_w$	wall temperature ( $^\circ\text{C}$ )
$T_s$	saturation temperature ( $^\circ\text{C}$ )
$\Delta X$	distance between thermocouples (mm)
$\delta$	uncertainty

## Subscripts

$\text{eff}$	effective
$\text{in}$	input
$\text{cu}$	copper

Kandlikar [7] used porous coatings in pool boiling experiment for increasing the nucleation sites. They found that porous coatings facilitate liquid flow through capillary pores which contribute significant increase in heat transfer performance.

Surface wettability plays a major role in bubbles formation and their release mechanism in pool boiling. During last several years several research works have reported the modification of surface wettability by applying hydrophilic, hydrophobic or nanowires coatings on the surface. Wu et al. [8] experimentally investigated nucleate boiling and CHF of water and FC-72 on hydrophilic coating of  $\text{TiO}_2$  on the heating surface. The  $\text{TiO}_2$  coated surface had high affinity towards water and the surface remained flooded with the liquid. They observed 50.4% and 38.2% increase in CHF for water and FC-72 respectively. Similar experiment and observation was reported by Takata et al. [9]. Several works [10–12] have reported the combined effect of hydrophilic and hydrophobic surfaces on nucleate boiling. Zupančič et al. [12] performed pool boiling experiment with a mixed patterned surface having micron size hydrophobic patches on a hydrophilic surface. They observed significant increase in heat transfer coefficient. Incorporation of nanowires at proper thermal conditions changes both topological and chemical properties of the surface due to oxidation of chemicals on the surface which affects the wettability of the surface. Yao et al. [13,14] fabricated nanowires in heating surface by etching process which showed better heat transfer performance due to enhancement in surface wettability. Presence of nanowires in microchannels increased the overall heat transfer coefficient. The combination of nanowires and structured microchannel in pool boiling surface increases the surface wettability rendering the surface more hydrophilic, thus improving its CHF limit as compared to structured microchannels surface without nanowires. Inclusion of micro/nano structures in a heating surface increases both heat transfer coefficient and CHF limit due to (i) high surface roughness (ii) low thermal resistance because of thin layers of coating. The heating surface also experiences low thermal stress as it doesn't allow the heat to be accumulated on the surface. As soon as the heat is generated it gets removed from the surface, due to which the temperature difference between the surface and surroundings is very less resulting in low thermal stress, and better durability [15–17].

During pool boiling, uninterrupted liquid supply and removal of vapor bubbles from the nucleating region facilitate heat transfer mechanism and increase the CHF. Jaikumar and Kandlikar [18] modified a heating surface by incorporating separate channels for nucleating bubbles and separate feeder channels for liquid supply. They observed significant increase in heat transfer coefficient and CHF limit. The advantage of such surface is that continuous liquid supply to nucleate sites is possible which enhances the heat transfer performance.

Enhanced surface area for heat transfer, uninterrupted liquid supply to nucleate sites and favorable bubble departure mechanisms are key factors for enhancement of heat transfer coefficient and critical heat flux in pool boiling.

In present work a new configuration of microchannels structured surface is introduced in pool boiling to enhance heat transfer area and also to facilitate rewetting of heating surface. The heating surface is modified to a segmented finned microchannels structured surface. In this configuration both primary and secondary channels are fabricated on the heating surface to facilitate the coolant liquid supply to nucleating sites. Our group has already extensively investigated the performance of segmented finned microchannels in flow boiling and observed the better performance compared to uniform and diverging microchannels [21–24]. The objective of the present work is to investigate the performance of segmented finned microchannels structured surface in pool boiling heat transfer. The performance of segmented finned microchannel structured (SF) surface has been compared with the uniform cross-section microchannels structured (UCS) and plain surface. Further present results have been compared with the available experimental results of pool boiling with structured surfaces.

## 2. Experimental setup

### 2.1. Components of the experimental setup

An experimental setup has been developed for performing pool boiling experiment. The schematic view of the experimental setup has been shown in Fig. 1. Main components of the setup are: boiling vessel, test module, thermocouples, AC power source, high speed camera and high speed data acquisition system. A cylindrical vessel made of borosilicate glass with diameter 150 mm and height 300 mm has been used to store liquid pool. Pool boiling experiment was performed with deionized water. The test module housing the heating surface has been fitted into the boiling vessel from the bottom side and heating surface was kept in horizontal position during experimentation. The boiling chamber was covered by a lid with a small hole at the center of the lid. Thus the chamber is partially open to the ambient for vapor venting. Similar types of chamber for pool boiling experiments have been reported in the literature [14,25].

A silicone rubber band heater of 600 W was used as an auxiliary heater to maintain the saturation temperature of water in the reservoir. Temperature of heating surface and water were measured using five numbers of K-type thermocouples. Three thermocouples  $T_1$ ,  $T_2$  and  $T_3$  have been used to measure heating surface temperature whereas two thermocouples  $T_4$  and  $T_5$  have been used

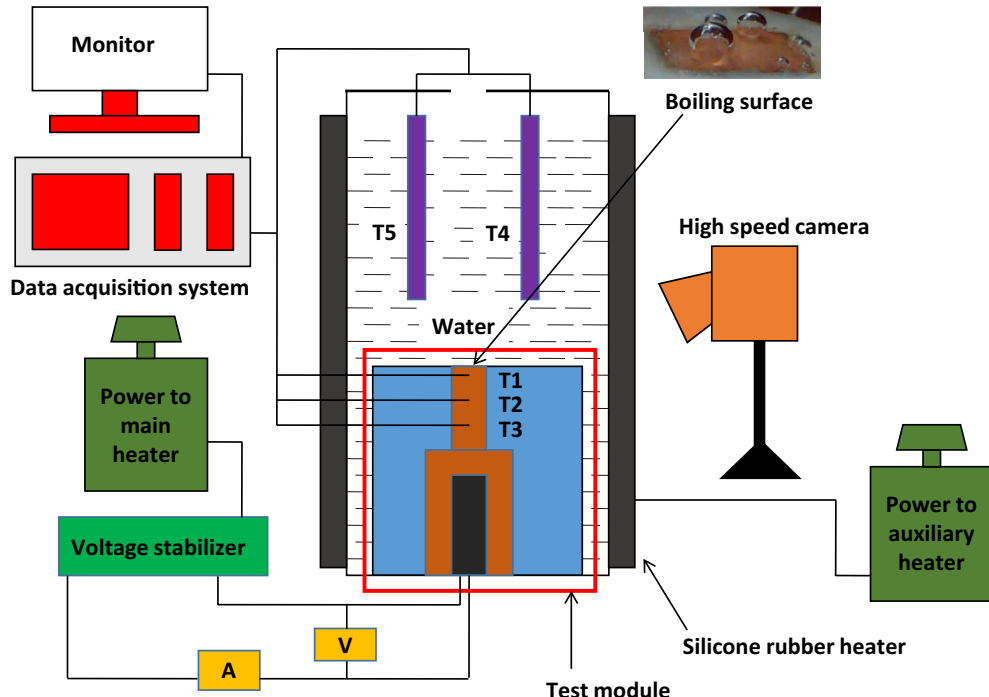


**Fig. 1.** Schematic view of experimental setup.

to measure the water temperature inside the reservoir as shown in Fig. 1. Two variable sources of AC power supply (0–270 V and 10 A) have been used for main heater (inserted into the copper substrate) and the other for auxiliary heater. A high speed camera (Make: phantom v 7.3) has been used to capture flow patterns during pool boiling. In order to maintain better resolution, images have been captured with comparatively slow frame rate of 1000 frames per second at the resolution of  $800 \times 600$  pixels. A high speed data acquisition system (Make: National Instruments) interfaced with LabView software has been used to capture the experimental data.

## 2.2. Test module

The test module consists of a copper block and a Teflon block. The copper block is square shaped ( $10 \times 10 \text{ mm}^2$  cross-section

area) in top part and cylindrical (20 mm diameter) in bottom part as shown in Fig. 2. A central hole of 6 mm diameter is made in the cylindrical part of the block to insert the cartridge heater. Three micro drills at 3 mm apart are made at one face of the square part of the copper block to insert thermocouples. Heating surface is fabricated on the top surface of the copper block. The foot print area of heating surface for all three configurations has been kept as  $10 \times 10 \text{ mm}^2$ . A high wattage density cartridge heater of 250 W capacity with 5.9 mm diameter and 25 mm length has been inserted into the copper block to apply heat to the heating surface. Three K-type thermocouples equally spaced at 3 mm apart have been used to measure the temperature gradient on the copper surface which is needed to measure the heating surface temperature. The copper block is insulated by a Teflon block which is cut to match the geometry of the copper block. To ensure a leak proof joint between the copper block and housing Teflon block a high temperature

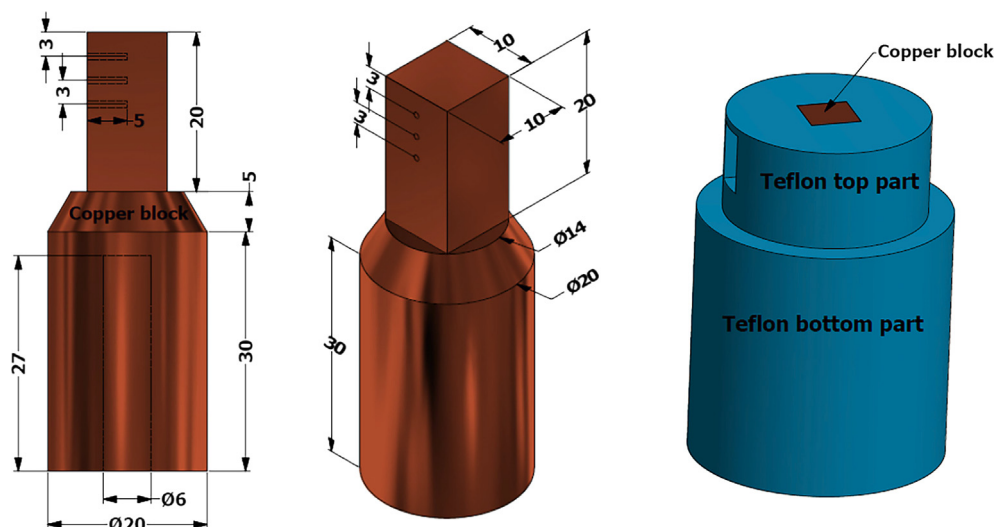


**Fig. 2.** Test module and exploded view of Teflon block (all dimensions are in mm).

resistant silicone sealant was used between them. The copper block and exploded view of Teflon block are shown in Fig. 2.

### 2.3. Heating surface configurations

In the present work pool boiling experiments have been performed with three different configurations of heating surfaces. Three different types of heating surfaces are: plain surface, uniform cross-section microchannels structured (UCS) surface and segmented finned microchannels structured (SF) surface.

All heating surfaces are made from the copper blocks of 99.99% purity. A foot print area of  $10 \times 10 \text{ mm}^2$  has been used for heating surface in each surface configuration as shown in Fig. 2. Both the microchannels structured surfaces have been fabricated using a micro-milling machine. The cross-section area of microchannel is  $400 \times 450 \mu\text{m}^2$  (width is  $400 \mu\text{m}$  and depth is  $450 \mu\text{m}$ ) and fin width is  $200 \mu\text{m}$ . The dimensions used in structured surfaces of the present work have been fixed based on the similar work reported in the literature. Cooke and Kandlikar [4] performed pool boiling experiments with microchannel structured surface by varying different dimensions i.e. channel width, height and fin width. Based on experimental investigation they observed the optimized heat transfer coefficient for channel depth more than  $400 \mu\text{m}$ , channel width more than  $350 \mu\text{m}$  and fin thickness  $200 \mu\text{m}$ . Present dimensions of UCS have been chosen based on their study. In segmented finned microchannels besides primary channels along the length of the surface, secondary channels or cross channels are cut inclined at an angle of  $30^\circ$  to the primary channels. Dimensions of both primary and secondary channels are equal and same as those of uniform cross-sectioned microchannels so that hydraulic diameter is same for both the structured surface

configurations. Due to cutting of both primary and secondary channels, 204 complete and 17 partial rhomboid shaped elements are generated at the heating surface. The schematics and photographs of both the structured surfaces are shown in Fig. 3.

Different dimensions of microchannels array have been presented in Table 1. It also shows the surface area augmentation factor which is the ratio of actual area (wetted area) of the surface to the projected surface area i.e. surface area of plane surface. Both the structured surfaces have nearly the same area enhancement. The dimensions were cross checked by SEM image and the maximum deviation was found within  $\pm 10 \mu\text{m}$ . The dimensions of structured surfaces have been fixed based on the earlier work [4] reported for uniform cross-sectioned structured surface. At the bottom of the surface some roughness were present, these are the effect of the milling process, where the end mill created small roughness on the bottom of the surface and small burrs may present on the top the surface.

### 3. Experimental procedure

Deionized (DI) water has been used as the boiling liquid. Experiments have been performed at atmospheric conditions. Before starting the actual experiment, water was boiled vigorously for more than 20 min to remove the dissolved gases. It should be noted that degassing method adopted in the current work is prevalent in the literature of pool boiling investigations [3,4,14]. Due to escaping of dissolved gases and evaporation, certain amount of water was lost. Makeup water at same temperature as that of the bulk of the boiling liquid was added intermittently to replenish the evaporated water vapor. Before the experiment, the heating surfaces were first cleaned using HCl (36.46%) solution and then

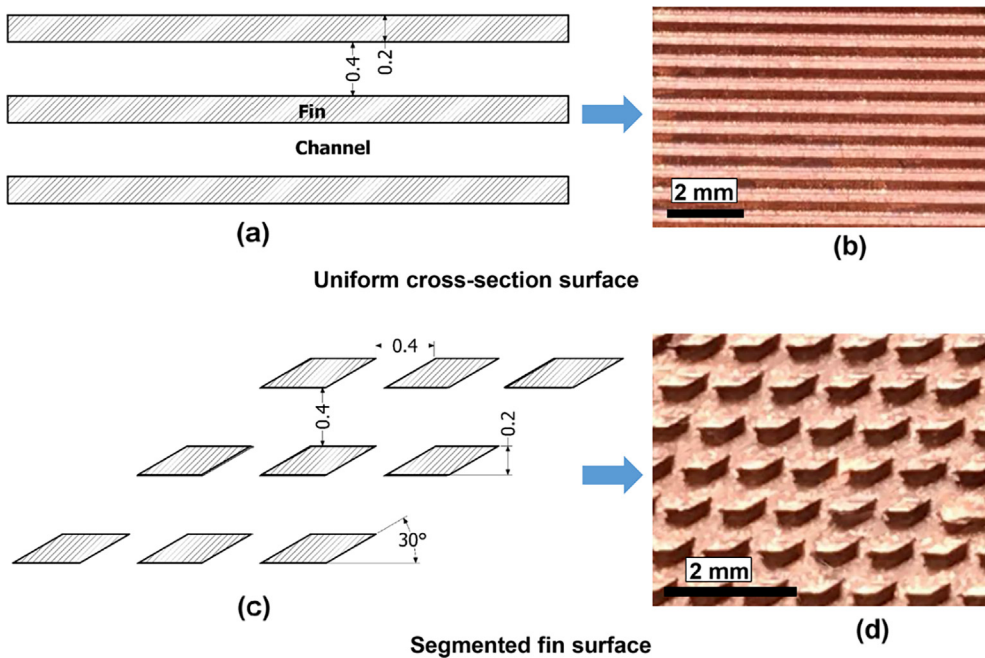


**Fig. 3.** Schematic and photograph of structured surfaces.

**Table 1**

Dimensions of microchannels in structured surfaces.

No.	Channel type	Length (mm)	$W_{ch}(\mu\text{m})$	$H_{ch}(\mu\text{m})$	$D_h (\mu\text{m})$	No. of channels	Surface area augmentation factor
1	UCS-Surface	10	400	450	554	17	2.53
2	SF-Surface	10	400	450	554	17	2.56

blow dried with nitrogen. The test surfaces are again rinsed gently in NaOH solution (0.1 mol/L) followed by blow dried with nitrogen. Finally they were rinsed with DI water and then again blow dried with nitrogen. Auxiliary heater was switched on throughout the experiment to maintain the water at saturation temperature. Voltage input to main cartridge heater was controlled by a variable transformer, and was adjusted from 0 to higher values of voltage in step of 10 V to obtain desired heating power. Experiments have been performed for effective heat flux in the range of 0–200 W/cm<sup>2</sup> based on the projected area of the heating surface. Heat transfer performance of all three surfaces was checked after the steady has been reached. Steady state has been assumed to reach when the temperature variation at a point was less than 0.25 °C per minute. For entire heat flux range, SF surface needed 15–20 min, UCS surface needed 20–25 min and plane surface needed 25–30 min to reach the steady state.

### 3.1. Calculation of heat flux

Heat transfer coefficient (HTC) during pool boiling experiments has been calculated based on effective heat flux ( $q''_{\text{eff}}$ ) which is the difference between total applied heat flux and heat loss. Total heat input ( $q_{\text{in}}$ ) to the test section is calculated based on the electric voltage (V) and current (I) supplied to the heater.

$$q''_{\text{in}} = \frac{VI}{\text{Area}} \quad (1)$$

The effective heat flux was calculated based on the temperature gradient observed in the copper block below the heated surface. The temperature gradient was calculated using three point's backward finite difference method as given below.

$$\frac{dT}{dX} = \frac{3T_1 - 4T_2 + T_3}{2\Delta X} \quad (2)$$

In above  $T_1$ ,  $T_2$  and  $T_3$  are temperatures measured by three thermocouples attached to the copper block as shown in Fig. 1. Based on the temperature gradient, the effective heat flux is calculated as follows:

$$q''_{\text{eff}} = k_{\text{cu}} \frac{dT}{dX} \quad (3)$$

The amount of heat loss during experiment was estimated from the difference of total input heat flux and effective heat flux.

$$q''_{\text{loss}} = q''_{\text{in}} - q''_{\text{eff}} \quad (4)$$

Based on the above methods, the heat loss was found to be within 5–10% of the applied heat for the entire range of heat flux. The wall superheat was calculated by:

$$\Delta T = T_w - T_s \quad (5)$$

Based on the effective heat flux and wall superheat, the heat transfer coefficient has been calculated as:

$$h = \frac{q''_{\text{eff}}}{\Delta T} \quad (6)$$

### 3.2. Uncertainty analysis

In order to check the accuracy of present experimental technique, all the sensors and measurement systems are calibrated. The maximum uncertainties in the thermocouples were found to be ± 0.5 °C. The uncertainties associated with other measurements have been calculated using standard error analysis [26]. The uncertainties in various quantities are calculated in the following manner:

### Uncertainty in effective heat flux ( $q''_{\text{eff}}$ )

$$\frac{\delta q''_{\text{eff}}}{q''_{\text{eff}}} = \left[ \left( \frac{\delta(\Delta T)}{\Delta T} \right)^2 + \left( \frac{\delta(\Delta X)}{\Delta X} \right)^2 \right]^{\frac{1}{2}} \quad (7)$$

### Uncertainty in heat transfer coefficient ( $h$ )

$$\frac{\delta h}{h} = \left[ \left( \frac{\delta q}{q} \right)^2 + \left( \frac{\delta(\Delta T)}{\Delta T} \right)^2 \right]^{\frac{1}{2}} \quad (8)$$

The average uncertainties in effective heat flux ( $q''_{\text{eff}}$ ) and heat transfer coefficient ( $h$ ) are observed as ± 5.3 W/cm<sup>2</sup> and ± 0.9 W/cm<sup>2</sup>K respectively.

## 4. Results and discussions

In this section the results of pool boiling experiments performed with three different heating surfaces have been presented and their performances have been compared. Results are expressed in terms of effective heat flux, wall superheat and heat transfer coefficient. Pool boiling heat transfer performance depends on the wettability characteristics of the heating surface. Surface wettability characteristics of three different configurations of heating surfaces used in the present experiment have also been analyzed.

### 4.1. Surface wettability

Surface wettability plays an important role in boiling heat transfer coefficient and critical heat flux (CHF). Several works [8,9,14–16,27] have reported the different techniques of surface wettability enhancement such as surface coating with hydrophilic materials, growing nanowires or carbon nanotubes on the heating surface. Besides all these techniques, surface wettability can also be changed by incorporating micro level roughness in the heating surface which has been undertaken in the present work. It should be noted that compared to different techniques of lithography, chemical etching or deposition, present technique of fabricating structured microchannels on a heating surface is simple and less time consuming. All those techniques require multi-tasks and different types of sample preparation are needed, whereas microfabrication process is a single step technique. Before measuring the contact angles, the test surfaces were cleaned as described in Section 3.

Wettability characteristics of all three surfaces have been evaluated by placing a water droplet and recording the droplet spreading phenomenon with the help of high speed camera. The static contact angle has been calculated by analyzing the image with the help of Image J software. Wettability of a surface depends on the surface energy of the material [28] and copper used in the present work does not change the surface energy in room temperature. The intrinsic contact angle of a smooth surface depends on the interfacial properties of materials whereas apparent contact angle of a textured surface can be changed due to presence of surface roughness.

Roughness of the all surfaces has been measured with optical microscope and found to be 0.44 μm for plane surface, whereas roughness of the two structured surfaces has been found as 1.02 μm respectively. Contact angles of all the surfaces have shown in Fig. 4 and presented in Table 2. The plane surface shows a contact angle of 70°. For UCS structured surface, the value of contact angle in X and Y direction is observed as 130° and 66° respectively, whereas for SF structured surface, the value of contact angle is 0° for both the directions. It should be noted that measured contact angles of structured surfaces can be considered using imbibition

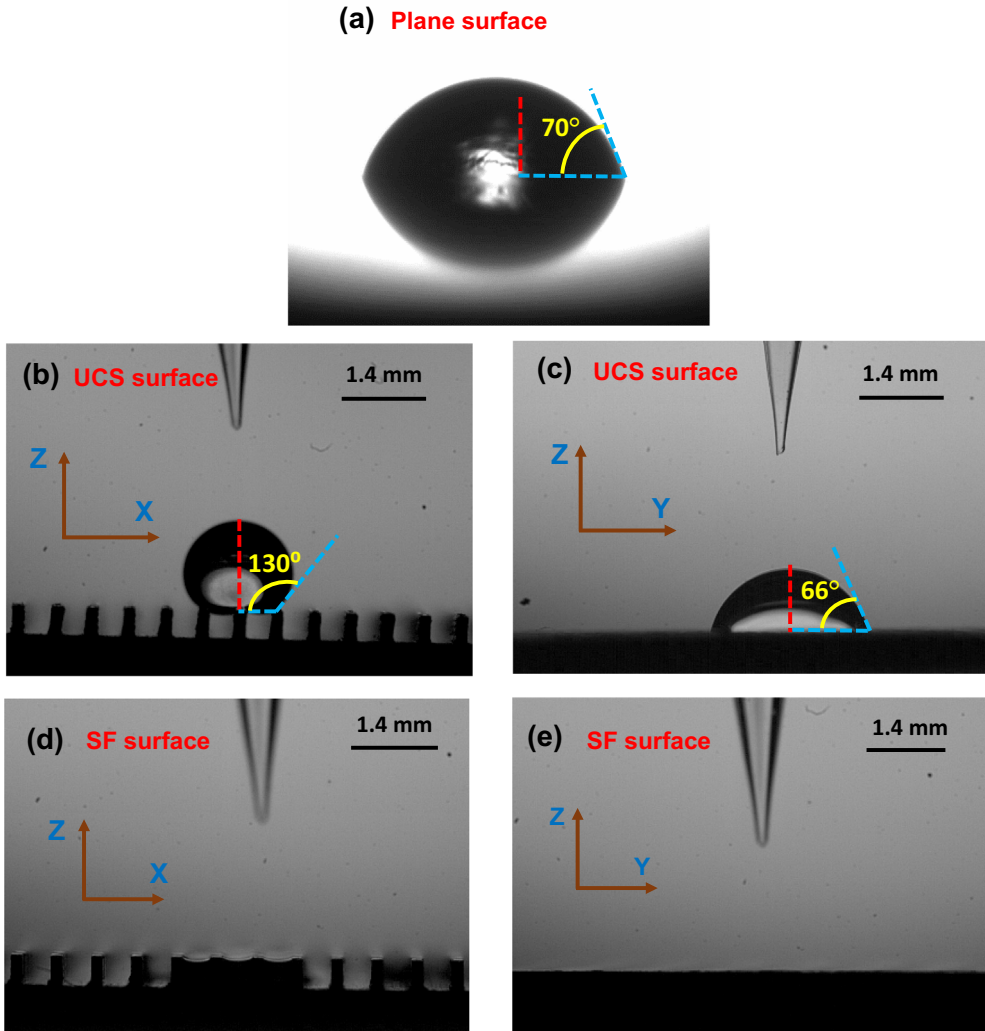


**Fig. 4.** Snapshots of the droplet spreading, (a) Plane surface,  $\theta = 70^\circ$  (b) UCS structured surface along X-direction,  $\theta = 130^\circ$ . (c) UCS structured surface along Y-direction,  $\theta = 66^\circ$ , (d and e) SF structured surface  $\theta \sim 0^\circ$  along X and Y direction.

**Table 2**  
Values of contact angle in plane and structured surface.

No.	Types of surface and direction	Contact angle
1	Plane surface	$70^\circ$
2	UCS(X direction)	$130^\circ$
	UCS(Y direction)	$66^\circ$
3	SF (both X and Y direction)	$\sim 0^\circ$

condition developed by Chung et al. [29]. Contact angle of textured surface for imbibition condition is given as:

$$\cos\theta_{imb} = \frac{1-f}{r-f} \quad (9)$$

where  $f$  represents the projected area of the solid surface that is wetted by the liquid and  $r$  represents the ratio of total surface area of the textured surface to its projected area. The values of  $f$  for UCS and SF surface have been obtained as 0.333 and 0.166 respectively whereas values of  $r$  have been obtained as 2.53 and 2.56 for UCS and SF surface respectively. Based on these the value of  $\theta_{imb}$  for UCS and SF surface has been obtained as  $72^\circ$  and  $70^\circ$  respectively. Since contact angle for plane surface is less than or equal to contact angle for imbibition, the droplet should spread in both the textured surfaces. In case of SF surface the droplet spreads through and across the

microchannels, showing a completely wetting behavior. On the other hand in case of UCS surface, the droplet gets pinned between the fins of microchannels in the X-direction, thus prohibiting it from spreading, which results in a high contact angle of  $130^\circ$ . Whereas the droplet spreads in the Y-direction because of low energy barrier thereby showing a low contact angle of  $66^\circ$ . Thus it shows like a rectangular bubble as reported by Chung et al. [29]. It should be noted that Yao et al. [14] also observed the hydrophilic behavior of nano-structured microchannels. However they observed high values of contact angles in microchannels structured surface in X- and Y- direction.

#### 4.2. Reliability and repeatability test of experimental setup

The reliability of present experimental facility was checked by comparing present results with available experimental data. Present experimental data of critical heat flux during pool boiling of water with plain surface have been compared with two empirical correlations developed by Lienhard and Dhircorrelation [30], and Zuber [31]. Empirical correlation of critical heat flux proposed by Lienhard and Dhircorrelation [30] is given as:

$$q^{critical} = 0.149 h_{fg} \rho_v^{\frac{1}{2}} [\sigma g (\rho_l - \rho_v)]^{\frac{1}{4}} \quad (10)$$

Whereas empirical correlation of critical heat flux developed by Zuber [31] is given as:

$$q_{\text{critical}}^{\text{critical}} = 0.131 h_{fg} \rho_v \left[ \frac{\sigma g (\rho_l - \rho_v)}{\rho_v^2} \right]^{\frac{1}{4}} \quad (11)$$

The comparison of present results has been presented in Table 3. It can be seen that present results show a deviation of 12.7% with the results of Lienhard and Dhir correlation [30] whereas it shows a deviation of 4.89% with the correlation of Zuber [31]. It has also been found from the literature survey that several investigations [4,18] have reported CHF in the range 100–130 W/cm<sup>2</sup> for pool boiling of water with plain surface.

Thus present experimental facility is well validated. It should be noted that in the present work CHF has been attained only in plain surface. In case of structured surfaces before reaching CHF, excessive temperature was developed in the copper block and experiment was stopped to avoid the burning of the Teflon block.

In order to evaluate hysteresis loss and repeatability check, pool boiling experiments were performed with plain heating surface with increasing and decreasing heat flux. Fig. 5 shows the results of heat flux versus wall superheat. It can be seen that results show similar trend for both increasing and decreasing heat flux and there is no significant difference between the two cases.

This confirms that there is no hysteresis loss. Further repeatability of the experimental data was checked by performing the experiment on three different days and calculating heat transfer coefficients as presented in Fig. 6. It can be seen that experimental data produces repeatability quite well.

#### 4.3. Comparison of heat transfer performance

Fig. 7 shows the plot of heat flux versus wall superheat i.e. boiling curves for all three configurations of heating surface. Heat flux presented in the plot is based on the projected area of the heating surface. It can be seen from Fig. 7 that from very early stage both the structured surfaces show lower wall superheat compared to the plane surface. It is due to consideration of top fin surface for representing wall temperature in two structured surfaces. In the present work top fin surface has been used for representing wall temperature of two structured surfaces, whereas for plane surface wall temperature is calculated based on the heating surface itself. In order to measure the wall temperature, three thermocouples are embedded at 3 mm distance below from the top fin surface of two structured surface and at 3 mm distance below from the plane surface (see Section 2.2). This practice is adopted from the literature reported for similar pool boiling experiments with structured surface [3,4]. The depth of the channels in each structured surface is 450 μm. Thus fin top surfaces of structured surfaces are 450 μm above the base area of plane surface. So for similar operating conditions, wall temperatures of two structured surfaces are less than the plane surface which reduces the wall superheat. Nevertheless this initial wall superheat has no role in heat transfer characteristics of pool boiling in later on as pool boiling is affected by bubble dynamics in later stage and heat transfer coefficient can be represented by slope of the boiling curve.

It can be seen that boiling curve of segmented finned microchannels structured surface shows the highest slope with the lowest wall superheat whereas plain surface shows the lowest slope with highest wall superheat. The uniform cross-section microchannels structured surface shows the mediocre performance in between these two surfaces. Low wall superheat means

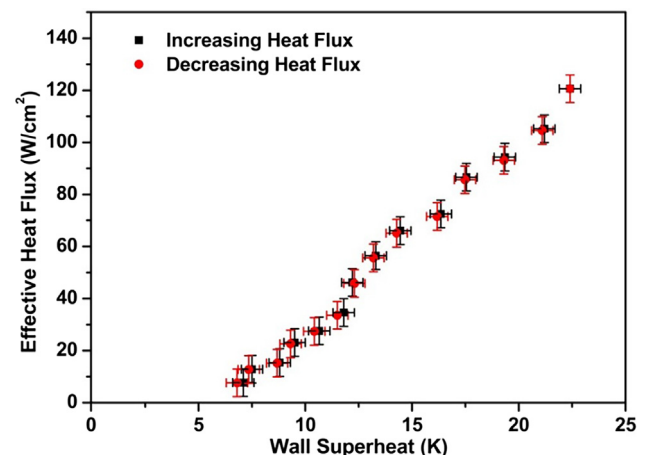


Fig. 5. Hysteresis plot for plain surface.

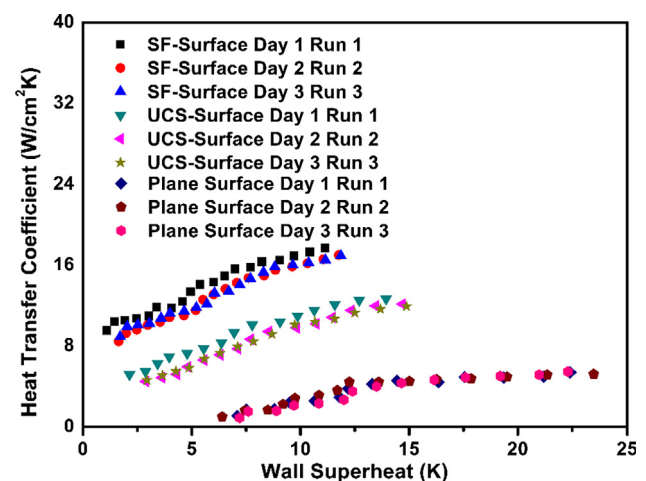


Fig. 6. Repeatability checking of experimental data.

high heat transfer coefficient. Thus segmented finned microchannels structured surface shows better performance than the performance of other two surfaces.

Comparison of pool boiling heat transfer coefficient in all three surface configurations has been shown in Fig. 8. It has been observed that for all surfaces heat transfer coefficient increases with the increase in wall superheat. As wall superheat increases, boiling is initiated and heat transfer is enhanced due to microconvection, microlayer evaporation, and the transient conduction involved in pool boiling. Segmented finned microchannels structured surface shows the highest heat transfer coefficient whereas plain surface shows the least heat transfer coefficient.

It can also be seen that starting from very low wall superheat, the SF surface shows higher heat transfer coefficient compared to other two surfaces. At very low wall superheat, only natural convection heat transfer occurs, the UCS and SF structured heating surface provide extra surface due to which heat transfer coefficient is more compared to the plane heating surface. Once the nucleate boiling is initiated, bubble dynamics is greatly affected by the side-

**Table 3**  
Comparison of experimental setup with some known correlations.

Sl. no	Correlations	Fluid	Surface material	Surface finish	P <sub>sat</sub> (kPa)	Correlation value (W/cm <sup>2</sup> )	Expt. value (W/cm <sup>2</sup> )	% deviation
1	Lienhard & Dhir [30]	Water	Copper	Smooth	101.3	107.0	120.63	12.7
2	Zuber [31]	Water	Copper	Smooth	101.3	115.0	120.63	4.89

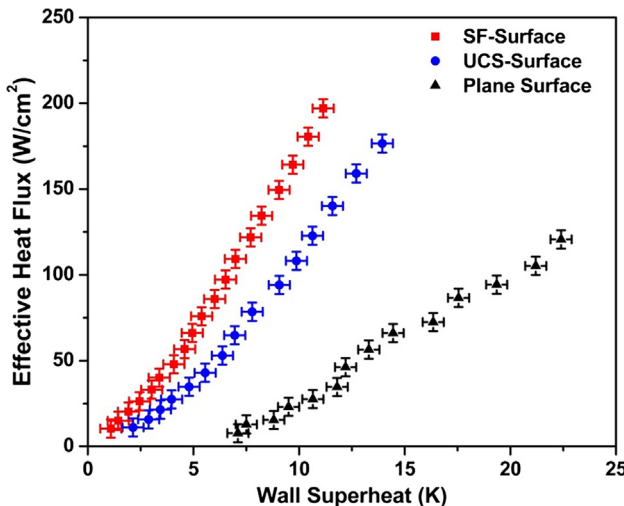


**Fig. 7.** Boiling curves for three surfaces with respect to projected area.

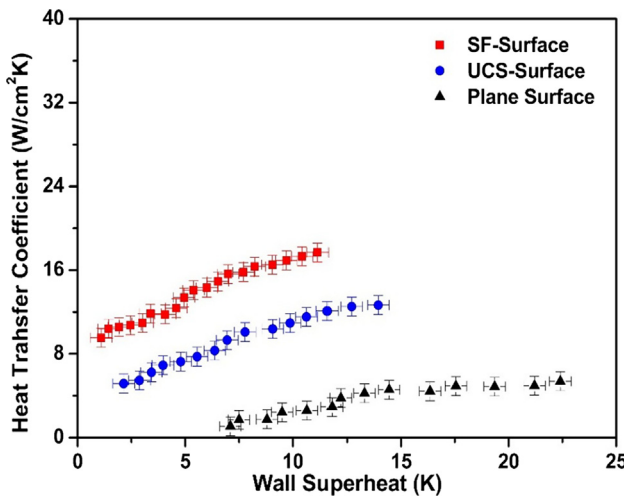


**Fig. 8.** Heat transfer coefficient vs. wall superheat of the test surfaces with respect to the projected area.

wall structures of UCS and SF surface. Micropillar structures present in SF surface provides active bubble nucleation sites. Moreover sharp corners in SF surface acts as active nucleation sites which decreases the nucleation temperature for heterogeneous nucleation [32] and hence increases the heat transfer coefficient. Thus heat transfer increases starting from initial stage.

Better heat transfer performance of SF structured surface may be attributed due to more nucleation site and favorable bubble dynamics compared to other two surfaces. Table 4 presents the heat transfer coefficient values of all three surfaces for heat flux of 120.63 W/cm<sup>2</sup>. It also presents the heat transfer enhancement factor of two structured surfaces. Comparing the area augmentation factor in Table 1 and heat transfer enhancement factor in Table 4, it can be observed that UCS structured surface exhibits

augmentation factor of 2.53 whereas its heat transfer enhancement factor is 2.5. The SF structured surface exhibits area enhancement factor almost equal to that of UCS, but it shows heat transfer enhancement factor of 3. Thus for the same area enhancement factor, SF structured surface performs better than UCS structured surface. Thus enhancement of surface area is not the sole reason for enhancing heat transfer rate in pool boiling. There must be role of bubble dynamics in heat transfer enhancement which has been discussed in next section.

#### 4.4. Comparison of bubble dynamics

Bubble dynamics and bubble ebullition cycle plays an important role in pool boiling heat transfer. Formation of nucleation sites, bubble formation, their growth and departure frequency affect the heat transfer performance in pool boiling. Bubble release mechanism and bubble release frequency from the heated surface largely affect the heat transfer mechanism. During pool boiling, uninterrupted liquid supply and removal of vapor bubbles from the nucleating region facilitate heat transfer mechanism and increase the critical heat flux. In order to show the different stages of bubbles behavior, bubble dynamics has been presented at different time. Figs. 9–11 show the flow visualization of pool boiling performed with the two structured surfaces at different time levels for three different applied heat fluxes of 10 W/cm<sup>2</sup>, 15 W/cm<sup>2</sup> and 20 W/cm<sup>2</sup>. Flow visualization of plane surface has been discarded because there were very less numbers of nucleation activities for such low values of applied heat fluxes. The top view snapshots captured by high speed camera at the time level of 10 min, 20 min and 30 min respectively have been presented here. Fig. 9 shows the bubble behavior at different time levels for applied heat flux of 10 W/cm<sup>2</sup>. In UCS structured surface few active nucleation sites are observed at the time level of 10 and 20 min respectively. Thus at low applied heat flux (10 W/cm<sup>2</sup>) numbers of growing bubbles in SF surface is more compared to the UCS surface. Micropillar structures present in SF surface provide active nucleation sites. Naturally such surfaces promote early nucleation and increase the bubble departure frequency. At 30 min few bubbles coalesce to form big bubbles which sizes are approximately equal to the channel width. In case of SF structured surface, nucleation starts much earlier and at the time level of 10 min bubbles grow to channels size. At 20 min bubbles grow from multiple sites and their sizes are slightly bigger than the channel size. At time level of 30 min multiple sizes of bubbles are formed at different locations and bubbles size becomes almost double of the channel size. Fig. 10 shows the bubble growth for applied heat flux of 15 W/cm<sup>2</sup>. Both structured surfaces show the active nucleation sites along the channel passages at time level of 10 min.

In case of SF surface some nucleation sites are observed along the secondary channels at 20 min. As the time progresses bubbles grow to bigger size in UCS structured surface compared to the SF structured surfaces which can be observed at the time level of 20 and 30 min. For applied heat flux of 20 W/cm<sup>2</sup> in case of UCS structured surface bubbles start nucleating at the channel passages and they coalesce to form bigger size as shown in Fig. 11. After nucleation at the bottom, the bubbles slide along the fin surface and in that process they coalesce with the nearby growing bubbles eventually forming a large bubble on the top of the microchannel.

During vigorous boiling in UCS surface, the bubble slug length increases along the channel passage (Y- direction), it obstructs the entry of fresh coolant and this makes it difficult for the surrounding liquid to rewet the surface. On the other hand fresh coolant cannot flow along X-direction due to presence of fins. In absence of rewetting phenomenon of nucleation sites, bubble grows explosively in UCS surface at high heat flux. On the other hand in case of SF structured surface, the growth rate of nucleating

**Table 4**  
HTC and enhancement factor based on plane surface for heat flux of 120.63 W/cm<sup>2</sup>.

No.	Type of Surface	h(W/cm <sup>2</sup> K)	Enhancement factor
1	Plane surface	5.385	–
2	UCS Surface	11.46	2.0
3	SF Surface	15.79	3.0

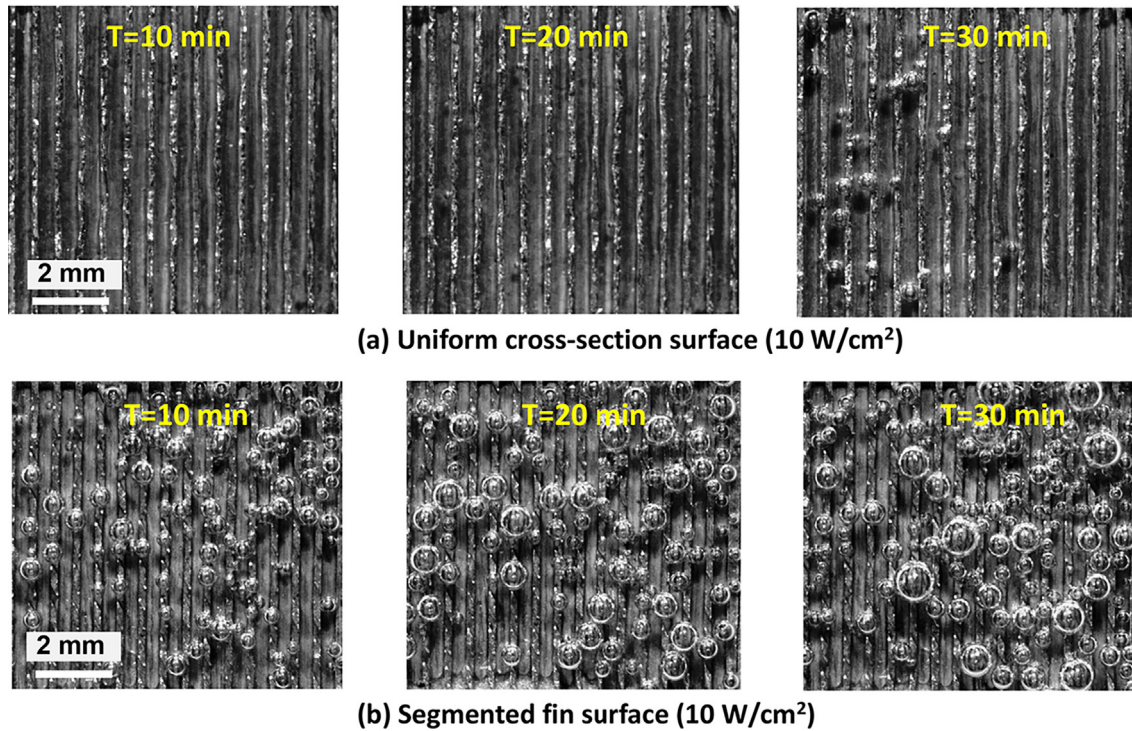


**Fig. 9.** Bubble behavior of structured surfaces for heat flux of 10 W/cm<sup>2</sup>.

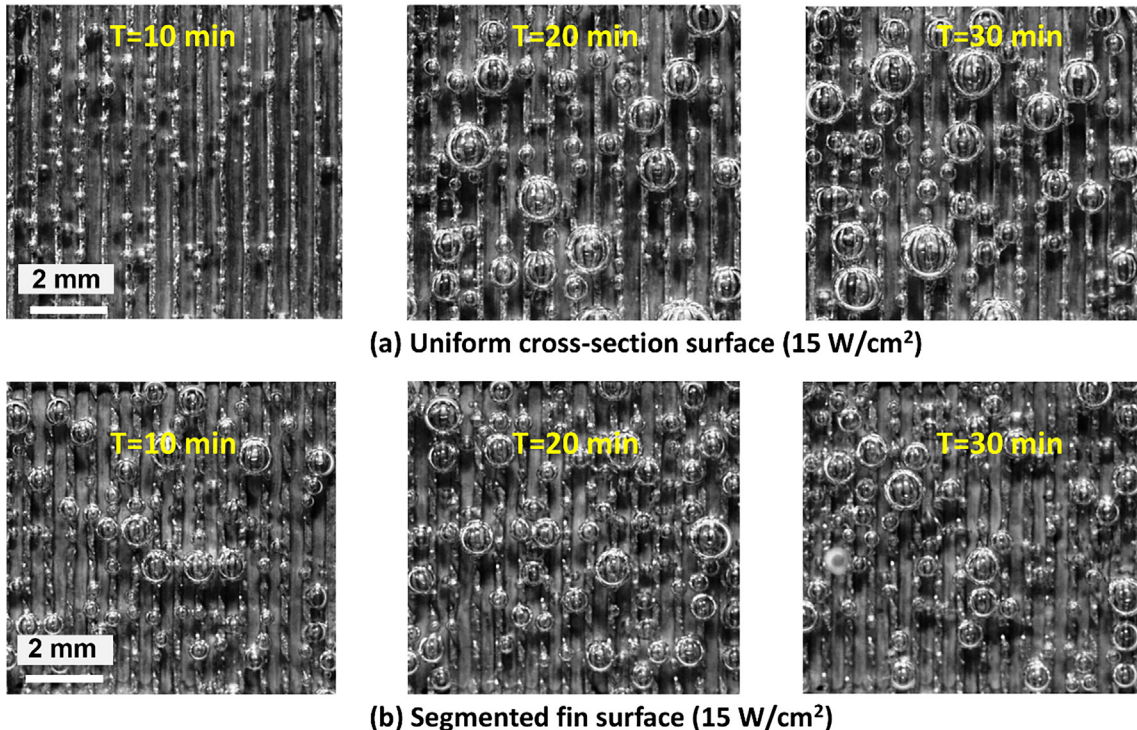


**Fig. 10.** Bubble behavior of structured surfaces for heat flux of 15 W/cm<sup>2</sup>.

bubbles is slower than UCS surface even though nucleation starts earlier. In this case because of capillary wicking and due to multiple pathways around the rhomboid micropillars, fresh liquid flows easily to replenish dry patches and prevents prolonged bubble coverage by pushing it away resulting in earlier detachment of bubbles. The mechanism of easy liquid replenishment and capillary

wicking delays CHF and also results in higher heat transfer coefficient. Thus segmented finned microchannel structure reduces bubble attachment time, which increases the bubble departure frequency and enhances the heat transfer.

Based on the flow visualization, a schematic view of the bubbles generation, their movement and rewetting of nucleation sites in SF

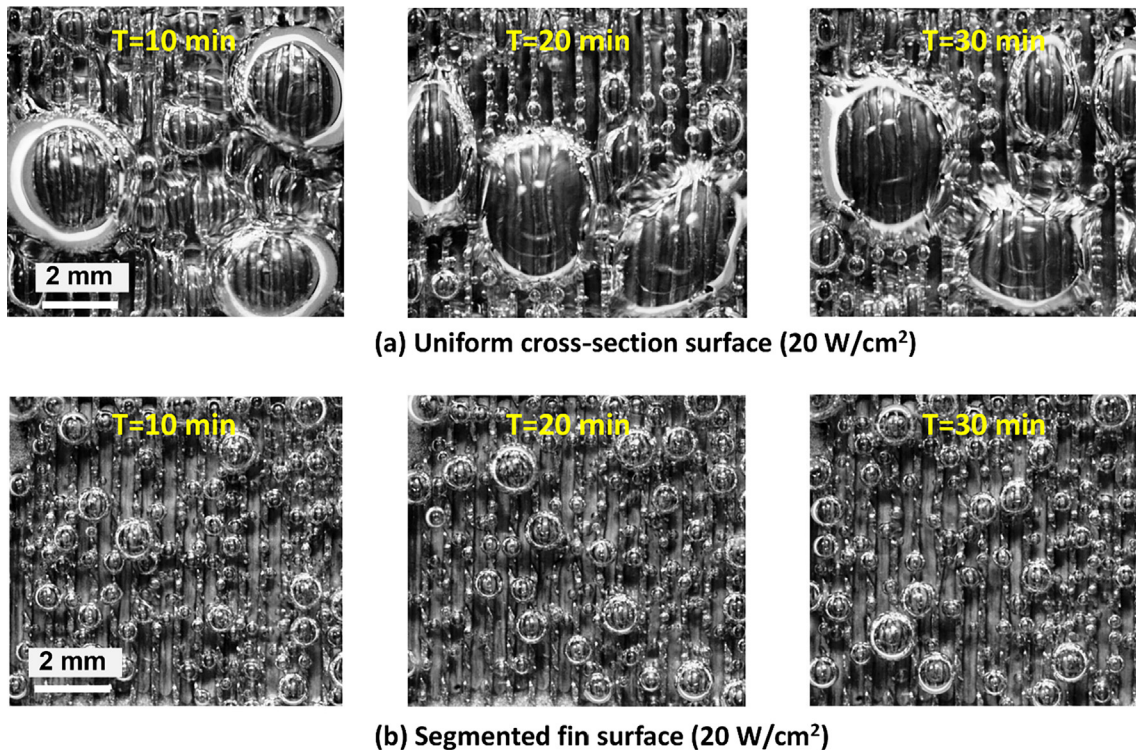


**Fig. 11.** Bubble behavior of modified surfaces for heat flux of  $20 \text{ W/cm}^2$ .

surface has been shown in Fig. 12. It has been observed that most of the bubbles nucleate from the bottom edges of the rhomboid elements and after nucleating they slide along the wall of the elements. As the bubbles slide along the fin edges, they grow and after reaching top of the fin surface they grow to the required size and then depart. On the other hand few nucleating bubbles coalesce together and grow at the bottom of the fin elements. These bubbles detach and depart directly to the bulk liquid without sliding along the fin walls. As soon as the bubbles nucleate, the fresh coolant enters through primary and secondary channels and rewet the surface below the nucleating bubble. Moreover fresh liquid can enter into the nucleating site from top under the influence of buoyancy circulation. Thus in this configuration transport of fresh liquid into the bubble nucleating site is possible from both vertical as well as horizontal direction as indicated by arrow mark in Fig. 12. In case of UCS surface, fresh liquid transport from the top side is possible. However liquid transport from side way in horizontal direction is not possible due to presence of fins in microchannels. In absence of proper rewetting phenomenon of nucleation sites, bubble grows explosively in UCS surface.

#### 4.5. Performance comparison with available experimental data

In the present work it has been already established that SF structured surface shows better pool boiling heat transfer performance compared to UCS structured and plain surface. In order to bench mark the present structured surface, its performance has been compared with available experimental data of pool boiling performed with different surface modification techniques. Present experimental results have been compared with available results reported in the literature for same operating conditions. Present experimental results have been compared with the results of Cooke and Kandlikar [4], Yao et al. [16], Shi et al. [27] and Wu et al. [8]. Cooke and Kandlikar [4] conducted pool boiling experiments with microchannels structured surface (Chip 8) having dimensions with the present surface. Present results have also been compared with the results of pool boiling performed with nanowires impinged surface (Yao et al. [16] and Shi et al. [27]) and surface coated with hydrophilic coating (Wu et al. [8]). Fig. 13 presents the comparison of boiling curve and Fig. 14 presents the comparison of heat transfer coefficient. It can be seen

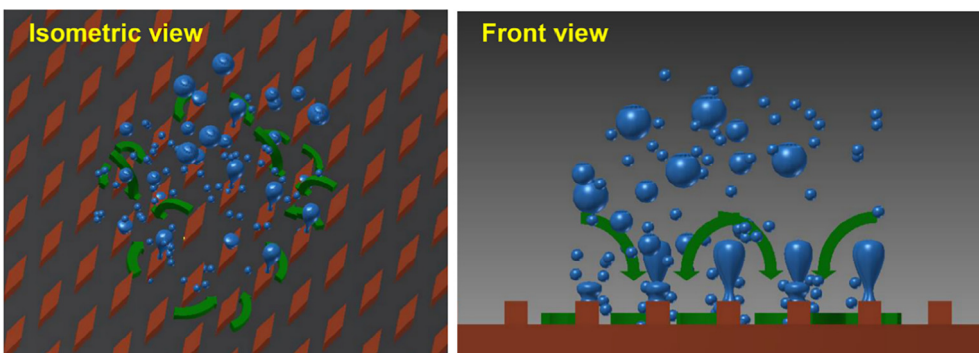


**Fig. 12.** Bubble dynamics in SF structured surface (not to scale).

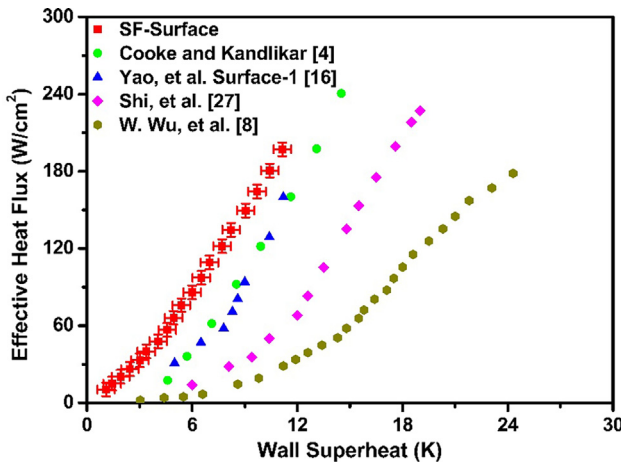


Fig. 13. Comparison of boiling curves with available data.

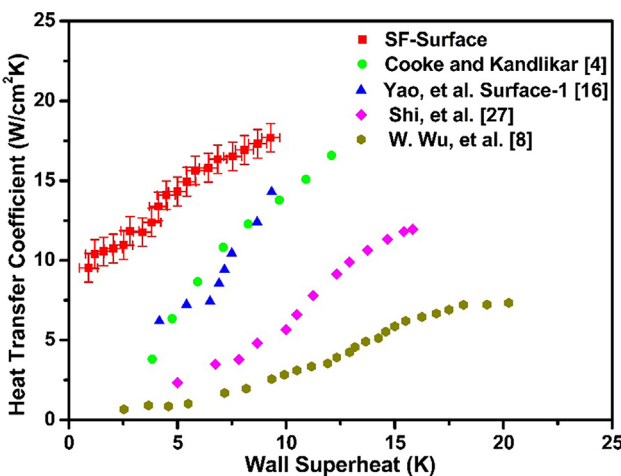


Fig. 14. Comparison of heat transfer coefficient with the available data.

that segmented finned microchannels structured surface shows the best heat transfer performance among all the surfaces. Table 5 present the comparison of present heat transfer coefficient with available experimental data for wall superheat of 10 °C. It also presents the ratio of the present HTC value to other available values. It can be seen that for same operating conditions heat transfer coefficient of SF structured surface is the largest among all surfaces.

Compared to complicated process of fabricating nanowires impinged surface, the fabrication of segmented finned microchannels structured surface is simpler whereas performance of later one is better than previous one. Thus even by simple and robust way of geometric modifications one can improve the surface texture and can achieve superior heat transfer performance in pool boiling, which can be eventually applicable for efficient electronics cooling applications.

**Table 5**  
HTC comparison of SF-Surface with available date for wall superheat of 10 °C.

Authors	Surface	HTC of present work (W/cm <sup>2</sup> K)	HTC reported from literature	Enhancement factor (HTC <sub>current study</sub> /HTC <sub>literature</sub> )
Current Study	SF-Surface	17.3	—	—
Cooke and Kandlikar [4]	Microchannel-Chip 8	—	12.4	1.4
Yao et al. [16]	Surface 1	—	12	1.44
Shi et al. [27]	Copper Nanowire	—	4.5	3.84
Wu et al. [8]	TiO <sub>2</sub> coated	—	2	8.65

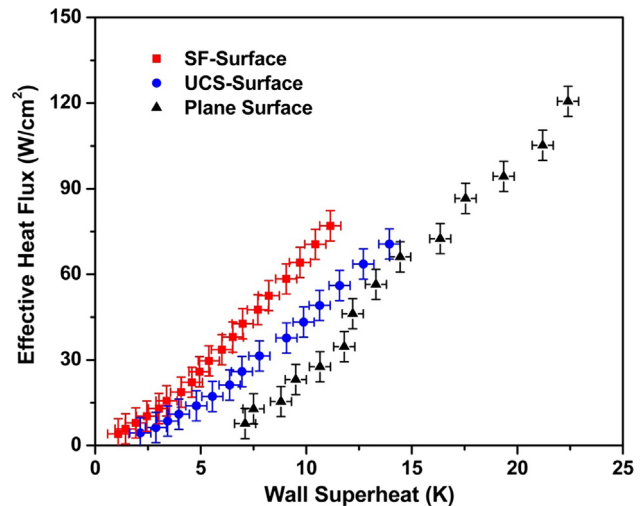


Fig. 15. Boiling curves with respect to actual surface area.

#### 4.6. Effect of actual surface area in heat transfer rate

It has already been discussed about the area enhancement due to fabrication of structured surfaces in heating surface. Surface augmentation factor has been presented in Table 1. In order to show the role of extra surfaces in structured surfaces the heat flux based on actual surface area (wetted area) has been calculated and comparison of boiling curves for all three surfaces have been presented in this section. Fig. 15 shows the plots of heat flux (based on actual area) versus wall superheat. Compared to Fig. 7 it can be seen that slopes of boiling curves of two structured surfaces have been decreased due to decrease in heat flux whereas slope of boiling curve of plane surface remains same. It is very interesting to observe that even after the boiling curve shifted down, slope of the segmented finned microchannel structured surface is higher than that of other two surfaces. It means that for same wall superheat the heat transfer coefficient is higher in segmented finned microchannels structured surface compared to other two surfaces. Further from the trend of boiling curve it can be expected that segmented finned microchannels structured surface would perform better and would also allow higher CHF than the other two surfaces.

#### 5. Conclusions

An experimental investigation has been performed to investigate the heat transfer characteristics of segmented finned microchannels structured surface in pool boiling and compare with the existing structured surface i.e. uniform cross-section microchannel structured surface and plain surface. Pool boiling experiments have been performed at normal atmospheric conditions using deionized water. The dimensions of both the structured surfaces were kept equal. Wettability characteristics of all three

surfaces have been evaluated. Segmented finned microchannels structured surface shows better wettability characteristics with contact angle nearly zero, whereas uniform cross-section microchannels structured surface has shown anisotropic wettability. Both the structured surfaces show almost equal area enhancement factor compared to plain surface. However segmented finned structured surface shows better heat transfer enhancement compared to uniform channels structured surface. Better bubble dynamics attributes the better heat transfer performance in segmented finned structured surface. At low heat flux nucleation started earlier and more numbers of nucleation sites were observed in segmented finned structured surface compared to uniform channels structured surface. In segmented finned configuration bubbles replacement from the nucleation sites was faster as rewetting phenomenon was effective due to transport of fresh liquid from both vertical as well as horizontal direction. From the comparison of present results with available experimental results, it has been observed that for similar operating conditions, segmented finned structured surface shows best performance.

## Appendix A. Supplementary material

Supplementary data associated with this article can be found, in the online version, at <https://doi.org/10.1016/j.ijheatmasstransfer.2018.06.115>.

## References

- [1] K. Chu, Y.S. Joung, R. Enright, C.R. Buie, E.N. Wang, Hierarchically structured surfaces for boiling critical heat flux enhancement, *Appl. Phys. Lett.* 102 (2013) 151602.
- [2] H. O' Hanley, C. Coyle, J. Buongiorno, T. McKrell, L.W. Hu, M. Rubner, R. Cohen, Separate effects of surface roughness, wettability, and porosity on the boiling critical heat flux, *Appl. Phys. Lett.* 103 (2013) 024102.
- [3] D. Cooke, S.G. Kandlikar, Pool boiling heat transfer and bubble dynamics over plain and enhanced microchannels, *J. Heat Transfer* 133 (2011) 052902-1–052902-9.
- [4] D. Cooke, S.G. Kandlikar, Effect of open microchannel geometry on pool boiling enhancement, *Int. J. Heat Mass Transfer* 55 (4) (2012) 1004–1013.
- [5] V. Umesh, B. Raja, A study on nucleate boiling heat transfer characteristics of pentane and CuO-pentane nanofluid on smooth and milled surfaces, *Exp. Therm Fluid Sci.* 64 (2015) 23–29.
- [6] R.J. Benjamin, A.R. Balakrishnan, Nucleation site density in pool boiling of saturated pure liquids: Effect of surface micro roughness and surface and liquid physical properties, *Exp. Therm Fluid Sci.* 15 (1) (1997) 32–42.
- [7] C.M. Patil, S.G. Kandlikar, Pool boiling enhancement through microporous coatings selectively electrodeposited on fin tops of open microchannels, *Int. J. Heat Mass Transfer* 79 (2014) 816–828.
- [8] W. Wu, H. Bostancı, L.C. Chow, Y. Hong, M. Su, J.P. Kizito, Nucleate boiling heat transfer enhancement for water and FC-72 on titanium oxide and silicon oxide surfaces, *Int. J. Heat Mass Transfer* 53 (9–10) (2010) 1773–1777.
- [9] Y. Takata, S. Hidaka, J.M. Cao, T. Nakamura, H. Yamamoto, M. Masuda, T. Ito, Effect of surface wettability on boiling and evaporation, *Energy* 30 (2–4) (2005) 209–220.
- [10] A.R. Betz, J. Jenkins, C.J. Kim, Daniel Attinger, Boiling heat transfer on superhydrophilic, superhydrophobic, and superbiphasic surfaces, *Int. J. Heat Mass Transfer* 57 (2) (2013) 733–741.
- [11] H.J. Jo, H.S. Ahn, S.H. Kang, M.H. Kim, A study of nucleate boiling heat transfer on hydrophilic, hydrophobic and heterogeneous wetting surfaces, *Int. J. Heat Mass Transfer* 54 (25–26) (2011) 5643–5652.
- [12] M. Zupančič, M. Steinbücher, P. Gregorčič, I. Golobi, Enhanced pool-boiling heat transfer on laser-made hydrophobic/superhydrophilic polydimethyl siloxane-silica patterned surfaces, *Appl. Therm. Eng.* 91 (2015) 288–297.
- [13] Z. Yao, Y.W. Lu, S.G. Kandlikar, Fabrication of nanowires on orthogonal surfaces of microchannels and their effect on pool boiling, *J. Micromech. Microeng.* 22 (2012) 115005 (9pp).
- [14] Z. Yao, Y.W. Lu, S.G. Kandlikar, Pool boiling heat transfer enhancement through nanostructures on silicon microchannels, *J. Nanotechnol. Eng. Med.* 3 (3) (2013) 031002-1–031002-8.
- [15] S. Ujereh, T. Fisher, I. Mudawar, Effects of carbon nanotube arrays on nucleate pool boiling, *Int. J. Heat Mass Transfer* 50 (19–20) (2007) 4023–4038.
- [16] Z. Yao, Y.W. Lao, S.G. Kandlikar, Direct growth of copper nanowires on a substrate for boiling applications, *Micro Nano Lett.* 6 (7) (2011) 563–566.
- [17] H.S. Ahn, N. Sinha, M. Zhang, D. Banerjee, S.K. Fang, R.H. Baughman, Pool boiling experiments on multiwalled carbon nanotube (MWCNT) forests, *J. Heat Transfer* 128 (12) (2006) 1335–1342.
- [18] A. Jaikumar, S.G. Kandlikar, Pool boiling enhancement through bubble induced convective liquid flow in feeder microchannels, *Appl. Phys. Lett.* 108 (2016) 041604.
- [19] P.C. Lee, C. Pan, Boiling heat transfer and two-phase flow of water in a single shallow microchannel with a uniform or diverging cross section, *J. Micromech. Microeng.* 18 (2008) 025005.
- [20] A. Kosar, Y. Peles, Thermal-hydraulic performance of MEMS-based pin fin heat sink, *J. Heat Transfer* 128 (2) (2005) 121–131.
- [21] Y.K. Prajapati, M. Pathak, Mohd. K. Khan, A comparative study of flow boiling heat transfer in three different configurations of microchannels, *Int. J. Heat Mass Transfer* 85 (2015) 711–722.
- [22] Y.K. Prajapati, M. Pathak, Mohd. K. Khan, Transient heat transfer characteristics of segmented finned microchannels, *Exp. Therm. Fluid Sci.* 79 (2016) 134–142.
- [23] Y.K. Prajapati, M. Pathak, Mohd. K. Khan, Bubble dynamics and flow boiling characteristics in three different microchannel configurations, *Int. J. Therm. Sci.* 112 (2017) 371–382.
- [24] Y.K. Prajapati, M. Pathak, Mohd. K. Khan, Numerical investigation of subcooled flow boiling in segmented finned microchannels, *Int. J. Heat Mass Transfer* 86 (2017) 215–221.
- [25] M.Q. Raza, N. Kumar, R. Raj, Surfactants for bubble removal against buoyancy, *Sci. Rep.* 6 (2016) 19113.
- [26] J.R. Taylor, An introduction to Error Analysis, University Science Books, Sausalito, California, 1997.
- [27] B. Shi, Y.B. Wang, K. Chen, Pool boiling heat transfer enhancement with copper nanowire arrays, *Appl. Therm. Eng.* 75 (2015) 115–121.
- [28] J.N. Israelachvili, Intermolecular and Surface Forces, Third Edition., Academic Press, 2011.
- [29] J.Y. Chung, J.P. Youngblood, C.M. Stafford, Anisotropic wetting on tunable micro-wrinkled surfaces, *Soft Matt.* 3 (2007) 1163–1169.
- [30] J.H. Lienhard, V.K. Dhir, Extended hydrodynamic theory of the peak and minimum pool boiling heat fluxes, NASA CR-2270, 1973, Contract No. NGL 18-001-035.
- [31] N. Zuber, On the stability of boiling heat transfer, *Trans. ASME* 80 (1958) 711–720.
- [32] J. Li, P. Cheng, Bubble cavitation in a microchannel, *Int. J. Heat Mass Transf.* 47 (2004) 2689–2698.